Density-matrix–electronic-oscillator representation of optical spectroscopy of semiconductor nanocrystals

S. Yokojima, T. Meier, and S. Mukamel
Department of Chemistry and Rochester Theory Center for Optical Science and Engineering, University of Rochester, Rochester, New York 14627

(Received 9 September 1996; accepted 9 December 1996)

The optical response of CdSe semiconductor nanocrystals is investigated using the reduced single-electron density matrix in real space, calculated by means of the time-dependent Hartree–Fock technique. The spectroscopic signatures of exciton confinement are analyzed using the frequency-dependent electronic coherence matrix (off-diagonal density-matrix elements). The effects of Hartree and the Fock (exchange) type Coulomb interactions on the exciton binding energy are discussed. The latter result in almost dark excitons situated energetically below the main transition. Off-diagonal Coulomb matrix elements lead to larger exciton binding energies compared with previous calculations, and result in a better agreement of the size dependence of the lowest optical transition with experiment. © *1997 American Institute of Physics.* [S0021-9606(97)03610-6]

I. INTRODUCTION

Studies of semiconductor nanocrystals in the size range of 10–100 Å are currently drawing a considerable experimental[1–23] and theoretical attention.[24–32] In spite of the similarity of their lattice structure to bulk semiconductors, nanocrystals possess dramatically different size-dependent electronic and optical properties. The confinement-induced quantization of the continuous bulk band-structure results in discrete electronic energy levels and a discrete optical spectrum, which is shifted towards higher energies with decreasing size.[5,6] Semiconductor nanocrystals constitute an ideal system for exploring systematically the evolution of material properties from molecular to bulk.[1–6] Numerous experimental studies of optical characteristics of semiconductor nanocrystals have been performed, yielding information about the size-scaling of electronic transitions, coupling with phonons, and optical nonlinearities. The linear absorption, has been studied in Ref. 7, and nonlinear measurements including three-pulse photon echo,[8,13] pump-probe,[14,17,18] Raman spectroscopy,[21] Stark spectroscopy,[11] fluorescence,[9,10,12,16,19,20,22,23] and electroluminescence[9,15] have been reported. Nanocrystals of various materials have been investigated including CdSe, CdS, CdTe, Si, and Ge.[6,16,21]

Many different theoretical techniques were developed and applied to investigate the optical properties of nanocrystals.[24–32] These can be classified into two main categories. The first, approach the nanocrystal from the bulk limit and make use of parameters obtained from the macroscopic band-structure. The effective mass approximation (EMA)[24,25] and the empirical pseudopotential method (EPM)[27,28] are the most widely used. In the second group, the nanocrystal is built microscopically out of individual atoms, and the coupling of their orbitals is considered explicitly. The starting point is then a tight-binding (TB) Hamiltonian,[29–32] and the nanocrystal is treated as a large molecule.

The EMA which only uses the bulk effective mass, works well for large nanocrystals in the vicinity of the fundamental band gap energy and predicts the observed trend of increased band gap for smaller sizes. For very small sizes, however, it significantly overestimates this effect. More rigorous extensions have introduced confined envelope wavefunctions for electrons and holes as well as the Coulomb interaction.[33] Nonparabolicities of the band-structures and effects due to valence band mixing have been included as well.[25,34] These lead to a better agreement of the calculated size-dependent band gap with experiment. Nonlinear optical properties have been investigated in Refs. 33 and 34. For small systems, however, the assumptions used in these models no longer hold.

The EPM has been first applied to semiconductor nanocrystals by imposing boundary conditions on the pseudopotential solution for the bulk.[27] In this method only the k-points determined by the infinite potential at the boundary are retained, resulting in a discrete spectrum. It is however impossible to apply this approach to investigate surface effects, and it is further restricted to simple nanocrystal shapes. These drawbacks were later overcome by introducing an empirical pseudopotential, which is continuous in momentum space, and allows to perform the calculation in real space.[28] Compared with the EMA, these methods give better agreement with observed size dependence of the exciton energies. However, the Coulomb interaction is not treated consistently in these models; to obtain the exciton energies, a Coulomb energy, which is inversely proportional to the system size, has been subtracted from the calculated single-particle energies.[27,28]

In contrast, calculations based on the TB approximation allow a fully microscopic study of the properties of the semiconductor nanocrystals in real space. These methods, which are tractable only for small sizes, provide an intuitive real-space physical picture, and are also well suited to incorporate surface effects, which are believed to strongly affect many

optical properties.[22,23,31] In the tight-binding (TB) models solved using a Green's function recursion[29,30] and the time-dependent checkerboard propagation[31,32] single-particle calculations showed the variation of the band gap and the density of states[29,30] with size. Most of these calculations, however, did not yield optical properties, such as the absorption spectrum, but only discussed the single-particle density of states.[29,31,32] In Ref. 30 the absorption spectrum of CdSe near the gap was calculated in the single-particle framework. Recently the electron-hole term of the Coulomb interaction has been included in the density of states calculation using a time-dependent technique.[32] So far no TB calculation of linear and nonlinear optical signals has been reported.

In this paper we develop the TB model to investigate the linear optical response of CdSe nanocrystals. Our approach is based on dynamical equations of motion for the reduced single-electron density matrix, derived using the time-dependent Hartree–Fock (TDHF) procedure.[35]

The TDHF was successfully applied to calculate linear and nonlinear optical properties of π-conjugated polyenes and inorganic semiconductors. In the polymer case, the Pariser–Parr–Pople (PPP) model was employed, where each carbon atom has a single π orbital. Using the TDHF framework, closed equations of motion for the reduced single-electron density matrix were derived, and successfully applied to investigate the optical properties.[36–41] Equations of motion developed for Frenkel exciton systems such as molecular aggregates reduce to the TDHF once the local-field approximation is made.[42] The TDHF thus allows a unified treatment of the optical response of semiconductor nanostructures, conjugated polyenes, and molecular aggregates.

Calculations of optical properties of inorganic semiconductors, are usually made using the semiconductor Bloch equations (SBE),[43–45] which are also based on the TDHF.[46] The SBE are dynamical equations for intra- and inter-band components of the density matrix, and their derivation relies on the distinction between electron and holes, i.e. on a band-structure calculation. Depending on the level of sophistication and the system studied, one may adopt a two-band (one valence and one conduction band) or a multi-band model. These equations have been solved for bulk semiconductors[46,47] and large semiconductor nanostructures.[48–50] Usually the calculations are performed in k-space, assuming an infinite system and homogeneous excitation. In our treatment we describe the nanocrystal directly in real space, considering explicitly the atomic orbitals and their couplings. We do not use confined wavefunctions, which would require a continuous interpolation of the real-space coordinates,[33,34] but rather work in the (discrete) site representation, which allows us to directly investigate the atomic charges and the coherences between electrons on different orbitals and atoms.

We apply our approach to CdSe nanocrystals using a model which includes 5 atomic orbitals (one s, three p, and one s^* orbital) on each atom.[51] The model includes two atoms and 8 valence electrons in a unit cell. In the bulk limit the 10 orbitals per unit cell result in 10 bands. We built an almost spherical nanocrystal by starting from a central atom and constructing n shells around it.[29,31] To calculate the ground state we consider the atomic energies and TB coupling between adjacent atoms. This model provides an adequate description of the highest valence bands and the lowest conduction band in a wide variety of materials.[51]

Using the TDHF scheme, we derive closed equations of motion for the reduced single-electron density matrix of our multiband model. These equations, which are similar to the multi-subband SBE used in the description of optical properties of semiconductor quantum wells[48,49] and superlattices,[50] can be used to calculate the linear as well as the nonlinear optical response of the nanocrystal. The direct (Hartree) and exchange (Fock) Coulomb interactions are properly included. Our numerical applications focus on the linear response where only the electron-hole part of the density matrix contributes. We study the size dependence of the lowest absorption feature. Our approach may be used to interpret the recently observed complexities of the optical transitions,[17] i.e., the many transitions show up in the linear absorption, due to the presence of multiple valence bands. The exciton fine structure[12,18] may be investigated as well. The Fock (exchange) interaction results in optically almost-forbidden excitons situated energetically below the main transition. Such low lying dark states should have a strong effect on the luminescence[52,53] by increasing the radiative lifetime. The nature of the luminescence is currently under active debate[12,20,52,53] and has important implications on electroluminescence in semiconductor nanoparticles. All of these effects can be studied directly in real space, using the density-matrix approach, which also allows us to investigate correlations between electrons on different atoms.

II. TIME EVOLUTION OF THE SINGLE-ELECTRON DENSITY MATRIX IN REAL SPACE

In this section we formulate the optical response of semiconductor nanocrystals using the real-space representation of the reduced single-electron density matrix and the TDHF scheme. Our theory starts with the Hamiltonian

$$\hat{H}=\hat{H}_0+\hat{H}_c+\hat{H}_{\rm int}, \tag{2.1}$$

where

$$\hat{H}_0=\sum_{\substack{i_1 i_2\\ \nu_1\nu_2}} T_{i_1 i_2}^{\nu_1\nu_2}\hat{c}_{i_1\nu_1}^{\dagger}\hat{c}_{i_2\nu_2}. \tag{2.2}$$

Here $\hat{c}_{i\nu}^{\dagger}$ ($\hat{c}_{i\nu}$) are the creation (annihilation) operators for electrons in orbital ν on atom i, which satisfy the Fermi anti-commutation relations;

$$[\hat{c}_{i_1\nu_1},\hat{c}_{i_2\nu_2}^{\dagger}]_+=\delta_{i_1 i_2}\delta_{\nu_1\nu_2}. \tag{2.3}$$

The diagonal elements $T_{ii}^{\nu\nu}$ represent the energy of an electron in orbital ν on site i, whereas the off-diagonal elements $T_{i_1 i_2}^{\nu_1\nu_2}$ are responsible for the hopping of an electron from orbital ν_1 on atom i_1 to orbital ν_2 on atom i_2. (For brevity, spin indices are included in the site indices i in this section.)

The second term represents the electron–electron Coulomb interaction:

$$\hat{H}_c=\frac{1}{2}\sum_{\substack{i_1i_2\\ \nu_1\nu_2\nu_3\nu_4}} V_1(^{\nu_1\nu_2\nu_3\nu_4}_{i_1i_2})\hat{c}^\dagger_{i_1\nu_1}\hat{c}^\dagger_{i_2\nu_3}\hat{c}_{i_2\nu_4}\hat{c}_{i_1\nu_2}. \tag{2.4}$$

The interaction between the electrons and the external electric field $\vec{E}$ is given by the third term in Eq. (2.1).

$$\hat{H}_{\rm int}=-\vec{E}(t)\cdot\sum_{\substack{i_1i_2\\ \nu_1\nu_2}}\vec{\mu}^{\nu_1\nu_2}_{i_1i_2}\hat{c}^\dagger_{i_1\nu_1}\hat{c}_{i_2\nu_2}, \tag{2.5}$$

where $\vec{\mu}$ is the dipole operator.

To investigate the dynamics of the system, we derive equations of motion for the reduced single-electron density matrix, defined by:

$$\rho^{\nu'\nu}_{ji}(t)\equiv\langle\Psi(t)|\hat{\rho}^{\nu'\nu}_{ji}|\Psi(t)\rangle, \tag{2.6}$$

where $|\Psi(t)\rangle$ is the total many-electron wavefunction, and the density matrix operator $\hat{\rho}$ is given by

$$\hat{\rho}^{\nu'\nu}_{ji}=\hat{c}^\dagger_{i\nu}\hat{c}_{j\nu'}. \tag{2.7}$$

The density matrix satisfies the Liouville equation:

$$i\hbar\frac{d}{dt}\rho^{\nu'\nu}_{ji}(t)=\langle\Psi(t)|[\hat{\rho}^{\nu'\nu}_{ji},\hat{H}]|\Psi(t)\rangle. \tag{2.8}$$

Once the Hamiltonian $\hat{H}$ (2.1) is inserted into (2.8), we find using (2.3) that four-point operators appear on the right hand side due to the many-particle Coulomb interaction. In order to close the equations, we assume that $|\Psi(t)\rangle$ may be represented by a single Slater determinant at all times (the TDHF approximation[35]). Then the four-point functions factorize into products of two-point single-electron densities:

$$\langle\Psi(t)|\hat{c}^\dagger_{i_1\nu_1}\hat{c}^\dagger_{i_3\nu_3}\hat{c}_{i_4\nu_4}\hat{c}_{i_2\nu_2}|\Psi(t)\rangle = \rho^{\nu_4\nu_3}_{i_4i_3}\rho^{\nu_2\nu_1}_{i_2i_1}-\rho^{\nu_4\nu_1}_{i_4i_1}\rho^{\nu_2\nu_3}_{i_2i_3}. \tag{2.9}$$

Using this factorization, we obtain the following closed equations for the elements of the reduced density matrix:

$$\begin{aligned}i\hbar\frac{d}{dt}\rho^{\nu'\nu}_{ji}(t)=&-\sum_{i_1\nu_1}T^{\nu_1\nu}_{i_1i}\rho^{\nu'\nu_1}_{ji_1}+\sum_{i_2\nu_2}T^{\nu'\nu_2}_{ji_2}\rho^{\nu_2\nu}_{i_2i}+E(t)\cdot\left(\sum_{i_1\nu_1}\vec{\mu}^{\nu_1\nu}_{i_1i}\rho^{\nu'\nu_1}_{ji_1}-\sum_{i_2\nu_2}\vec{\mu}^{\nu'\nu_2}_{ji_2}\rho^{\nu_2\nu}_{i_2i}\right)\\ &+\sum_{i_1\nu_1\nu_2\nu_3}\frac{1}{2}V_1(^{\nu_{11}\nu_2\nu_3\theta}_{i_1i})(\rho^{\nu_2\nu_3}_{i_1i}\rho^{\nu'\nu_1}_{ji_1}-\rho^{\nu_2\nu_1}_{i_1i_1}\rho^{\nu'\nu_3}_{ji})-\sum_{i_2\nu_1\nu_3\nu_4}\frac{1}{2}V_1(^{\nu_1\nu\nu_3\nu_4}_{ii_2})(\rho^{\nu_4\nu_3}_{i_2i_2}\rho^{\nu'\nu_1}_{ji}-\rho^{\nu_4\nu_1}_{i_2i}\rho^{\nu'\nu_3}_{ji_2})\\ &+\sum_{i_2\nu_2\nu_3\nu_4}\frac{1}{2}V_1(^{\nu'\nu_2\nu_3\nu_4}_{ji_2})(\rho^{\nu_4\nu_3}_{i_2i_2}\rho^{\nu_2\nu}_{ji}-\rho^{\nu_4\nu}_{i_2i}\rho^{\nu_2\nu_3}_{ji_2})-\sum_{i_1\nu_1\nu_2\nu_4}\frac{1}{2}V_1(^{\nu_1\nu_2\nu'\nu_4}_{i_1j})(\rho^{\nu_4\nu_1}_{ji_1}\rho^{\nu_2\nu}_{i_1i}-\rho^{\nu_4\nu}_{ji}\rho^{\nu_2\nu_1}_{i_1i_1}).\end{aligned} \tag{2.10}$$

We shall now define the Fock matrix h;

$$\begin{aligned}h^{\nu'\nu}_{ji}(\rho)=&T^{\nu'\nu}_{ji}+\frac{1}{2}\delta_{ji}\sum_{i_2\nu_3\nu_4}V_1(^{\nu'\nu\nu_3\nu_4}_{ii_2})\rho^{\nu_4\nu_3}_{i_2i_2}-\frac{1}{2}\sum_{\nu_2\nu_3}V_1(^{\nu'\nu_2\nu_3\nu}_{ji})\rho^{\nu_2\nu_3}_{ji}-\frac{1}{2}\sum_{\nu_1\nu_4}V_1(^{\nu_1\nu\nu'\nu_4}_{ij})\rho^{\nu_4\nu_1}_{ji}\\ &+\frac{1}{2}\delta_{ji}\sum_{i_1\nu_1\nu_2}V_1(^{\nu_1\nu_2\nu'\nu}_{i_1i})\rho^{\nu_2\nu_1}_{i_1i_1},\end{aligned} \tag{2.11}$$

and the Fock operator matrix corresponding to $H_{\rm int}$

$$f^{\nu'\nu}_{ji}(t)=-\vec{E}(t)\cdot\vec{\mu}^{\nu'\nu}_{ji}. \tag{2.12}$$

The equation of motion then assumes the following simple form, where all quantities represent matrices with a dimensionality equal to the basis set size (given by the number of sites times the number of orbitals per site)

$$i\hbar\frac{d}{dt}\rho(t)=[h(t)+f(t),\rho(t)]. \tag{2.13}$$

We next expand Eq. (2.10) in powers of the external field. To zeroth order we obtain the stationary Hartree–Fock equation,

$$[h(\overline{\rho}),\overline{\rho}]=0, \tag{2.14}$$

which determines Hartree–Fock ground state density matrix $\overline{\rho}$.

We then introduce $\delta\rho(t)$ ($\delta h(t)$) to denote the deviation of the time-dependent density matrix (Fock operator) from the ground state.

$$\rho^{\nu'\nu}_{ji}(t)=\overline{\rho}^{\nu'\nu}_{ji}+\delta\rho^{\nu'\nu}_{ji}(t), \tag{2.15}$$

$$h^{\nu'\nu}_{ji}(t)=h^{\nu'\nu}_{ji}(\overline{\rho})+\delta h^{\nu'\nu}_{ji}(t). \tag{2.16}$$

Equation (2.13) can then be recasted as

$$i\hbar\frac{d}{dt}\delta\rho=[h(\overline{\rho}),\delta\rho]+[f,\overline{\rho}]+[\delta h,\overline{\rho}]+[f,\delta\rho]+[\delta h,\delta\rho]. \tag{2.17}$$

Equation (2.17) can be used to compute the optical response to all orders in the optical field. In this paper we focus on the linear response; extension to the nonlinear response is briefly outlined in Appendix A. The last two terms on the right hand side of Eq. (2.17) are higher order in the field and do not affect the linear response. For the linear optical response, equation (2.17) then reads

$$i\hbar\frac{d}{dt}\delta\rho=[h(\overline{\rho}),\delta\rho]+[\delta h,\overline{\rho}]+[f,\overline{\rho}]. \tag{2.18}$$

The first two terms in Eq. (2.18) give the homogeneous part of the equation, whereas the third term describes the coupling to the external field. Writing these equations explicitly, including all the summations contained in the matrix structure of the quantities appearing in Eq. (2.18) results in

$$\begin{aligned}i\hbar\left(\frac{d}{dt}+\frac{1}{T_2}\right)\delta\rho_{ji}^{\nu'\nu}(t)=&-\sum_{i_1\nu_1}h_{i_1i}^{\nu_1\nu}(\overline{\rho})\delta\rho_{ji_1}^{\nu'\nu_1}+\sum_{i_2\nu_2}h_{ji_2}^{\nu'\nu_2}(\overline{\rho})\delta\rho_{i_2i}^{\nu_2\nu}+\vec{E}(t)\cdot\left(\sum_{i_1\nu_1}\vec{\mu}_{i_1i}^{\nu_1\nu}\overline{\rho}_{ji_1}^{\nu'\nu_1}-\sum_{i_2\nu_2}\vec{\mu}_{ji_2}^{\nu'\nu_2}\overline{\rho}_{i_2i}^{\nu_2\nu}\right)\\&+\sum_{i_1\nu_1\nu_2\nu_3}\frac{1}{2}V_1\binom{\nu_1\nu_2\nu_3\nu}{i_1i}(\delta\rho_{i_1i}^{\nu_2\nu_3}\overline{\rho}_{ji_1}^{\nu'\nu_1}-\delta\rho_{i_1i_1}^{\nu_2\nu_1}\overline{\rho}_{ji}^{\nu'\nu_3})-\sum_{i_2\nu_1\nu_3\nu_4}\frac{1}{2}V_1\binom{\nu_1\nu\nu_3\nu_4}{ii_2}(\delta\rho_{i_2i_2}^{\nu_4\nu_3}\overline{\rho}_{ji}^{\nu'\nu_1}\\&-\delta\rho_{i_2i}^{\nu_4\nu_1}\overline{\rho}_{ji_2}^{\nu'\nu_3})+\sum_{i_2\nu_2\nu_3\nu_4}\frac{1}{2}V_1\binom{\nu'\nu_2\nu_3\nu_4}{ji_2}(\delta\rho_{i_2i_2}^{\nu_4\nu_3}\overline{\rho}_{ji}^{\nu_2\nu}-\overline{\rho}_{i_2i}^{\nu_4\nu}\delta\rho_{ji_2}^{\nu_2\nu_3})-\sum_{i_1\nu_1\nu_2\nu_4}\frac{1}{2}V_1\binom{\nu_1\nu_2\nu'\nu_4}{i_1j}\\&\times(\delta\rho_{ji_1}^{\nu_4\nu_1}\overline{\rho}_{i_1i}^{\nu_2\nu}-\overline{\rho}_{ji}^{\nu_4\nu}\delta\rho_{i_1i_1}^{\nu_2\nu_1}).\end{aligned} \tag{2.19}$$

Here we have added a dephasing time T_2 which results in a Lorentzian line broadening of the calculated absorption spectra. Equation (2.19) fully determines the linear response and its solution provides all the information about the absorption spectrum as well as the nature of individual transitions (i.e., exciton wavefunctions, surface states, etc.). The Coulomb terms (V_1) couple of all components of the density matrix, which is reflected by the summations over the sites as well as the orbitals. These summations include the direct attractive (Hartree) Coulomb potential between electrons and holes, which leads to excitons, as well as the repulsive (Fock) exchange interaction. This second type of interaction, which is known to be negligible in the bulk limit[46,54] has been found to become more important with decreasing size.[12,18] In addition to the exchange interaction, we also include off-diagonal Coulomb-matrix elements (see Appendix B) which have been neglected in earlier treatments.[32] In the next section we show that this proper inclusion of the Coulomb interaction results in larger exciton binding energies and is a better agreement with experiment.

Equation (2.19) can be used to analyze the optical properties of nanocrystals over the entire size range all the way to the bulk. The standard Wannier-equation for the exciton[46,54] is recovered by neglecting the Fock-exchange terms, performing a continuous interpolation, transforming into relative and center-of-mass coordinates and assuming a homogeneous excitation, Eq. (2.19). In Appendices B and C we transform our equations to the molecular-orbital (MO) basis.[37] The standard bulk treatments are made using this basis and the analysis is sometimes more transparent in this representation. It should be emphasized that it is possible to separate the e-h part of the density matrix directly in real-space without transforming to the MO basis; within the TDHF this can be done simply by applying a commutator.[40]

III. APPLICATION TO CdSe NANOCRYSTALS

We have considered spherical semiconductor nanocrystals with 2, 3, 4, and 5 shells which have 17, 41, 83, 147 atoms, respectively. The center atom, which we call 0th shell, can be either Cd or Se. Se and Cd then appear alternately with increasing shell number until the surface atoms are reached. The coordinates were chosen as follows. The

TABLE I. The tight-binding parameters used for CdSe (in eV). We employ the notation of Ref. 31, which is evaluated by Lippens and Lannoo (Ref. 29) for the case of CdSe. The origin of this notation is in Refs. 51 and 55 which is based on Slater and Koster's (Ref. 61). We use the conventional notation in this tight-binding method, which is different from that of (2.2) by sign factors.

$T_{s(\mathrm{Se})s(\mathrm{Se})}$	−9.63
$T_{p(\mathrm{Se})p(\mathrm{Se})}$	1.47
$T_{s*(\mathrm{Se})s*(\mathrm{Se})}$	7.53
$T_{s(\mathrm{Cd})s(\mathrm{Cd})}$	0.03
$T_{p(\mathrm{Cd})p(\mathrm{Cd})}$	4.73
$T_{s*(\mathrm{Cd})s*(\mathrm{Cd})}$	5.72
$T_{s(\mathrm{Se})s(\mathrm{Cd})}$	−1.16
$T_{x(\mathrm{Se})x(\mathrm{Cd})}$	0.66
$T_{x(\mathrm{Se})y(\mathrm{Cd})}$	1.34
$T_{s(\mathrm{Se})p(\mathrm{Cd})}$	1.1425
$T_{p(\mathrm{Se})s(\mathrm{Cd})}$	1.385
$T_{s*(\mathrm{Se})p(\mathrm{Cd})}$	0.7625
$T_{p(\mathrm{Se})s*(\mathrm{Cd})}$	0.6225

TABLE II. Slater atomic orbitals for selenium ϕ^{Se} and for cadmium ϕ^{Cd} (in Bohr radius units).

ϕ^{Se}_{4s}	$0.685\,56\ r^{2.7}e^{-1.8784r}$	ϕ^{Cd}_{5s}	$0.046\,366\ r^{3}e^{-1.0875r}$
$\phi^{Se}_{4p_x}$	$1.187\,42\ r^{2.7}\sin\theta\cos\phi e^{-1.8784r}$	$\phi^{Cd}_{5p_x}$	$0.055\,059\ r^{3}\sin\theta\cos\phi e^{-r}$
$\phi^{Se}_{4p_y}$	$1.187\,42\ r^{2.7}\sin\theta\sin\phi e^{-1.8784r}$	$\phi^{Cd}_{5p_y}$	$0.055\,059\ r^{3}\sin\theta\sin\phi e^{-r}$
$\phi^{Se}_{4p_z}$	$1.187\,42\ r^{2.7}\cos\theta e^{-1.8784r}$	$\phi^{Cd}_{5p_z}$	$0.055\,059\ r^{3}\cos\theta e^{-r}$
ϕ^{Se}_{5s}	$3.8645\times10^{-5}r^{3}e^{-0.225r}$	ϕ^{Cd}_{6s}	$9.721\,649\times10^{-8}r^{3.2}e^{-0.0714r}$

center atom is located at the origin $(x,y,z)=(0,0,0)$. On the 1st shell 4 atoms are placed at $(a/4,-a/4,-a/4)$, $(-a/4,a/4,-a/4)$, $(-a/4,-a/4,a/4)$, and $(a/4,a/4,a/4)$. Here a is the lattice constant of CdSe which has a zincblende structure. The positions of all atoms in the 2nd and higher shells are uniquely determined by the zincblende structure. The structure of the system is thus uniquely specified by the number of atoms (or shells) and the type of the surface atoms (or the center atom). In the following, we denote the systems by the number of shells and the type of the surface atoms. For example, ''3-Cd'' denotes a nanocrystal with 3 shells (41 atoms) and Cd surface atoms (since the number of shells is odd, the center atom is Se in this case).

Surface atoms in nanocrystals have dangling bonds which strongly affect the optical spectra, by adding new absorption lines, some of which may be within the band gap.[31] In practice these bonds are usually passivated by an adsorbed species, and in order to compare with experiment they need to be removed. This is readily done by using sp^3 hybrid orbitals and an s^* orbital instead of the s, p and s^* orbitals. The transformation between the two sets of orbitals is given in Ref. 55. In a zincblende structure the hybrid orbitals point in the direction of the bonds: dangling bonds can be easily removed by simply eliminating the corresponding row and column from the Fock matrix.

The T matrix elements (Table I) have been obtained by fitting to the symmetry points of the band structure of bulk CdSe,[29,31,51] assuming that electron hopping occurs only between nearest neighbor atoms. We have used Slater's approximate analytical wavefunctions,[56] given in Table II and the resulting Coulomb integrals are given in Table III. The matrix elements of V_1 obtained using the monopole–monopole approximation are evaluated in Appendix D. The elements of the dipole operator, which can be evaluated analytically, are introduced in Appendix E and are given in Table IV.

In our ground state calculations we have neglected the Coulomb-terms in the Fock matrix $h(\overline{\rho})$. This was necessary, since we used single-electron TB parameters, which are known to reproduce the bulk band-structure.[29,31,51] Therefore T already takes into account some Coulomb interaction effects. If we include the full Coulomb interaction in the calculation of the TDHF equation (2.19), we would count parts of the Coulomb interaction twice. In calculating the ground state reduced density matrix Eq. (2.14), we therefore took T to be the stationary Fock matrix, that is,

$$h^{\nu'\nu}_{ji}(\overline{\rho})=T^{\nu'\nu}_{ji} \tag{3.1}$$

instead of Eq. (2.11).

We first calculated the density of states by diagonalizing the Fock matrices in (3.1). Figure 1 shows the results for the 2-, 3-, 4-, and 5-Se, and 2-, 3-, 4-, and 5-Cd crystals, respectively. The low energy peaks in the density of states, which can be seen around -12 eV, originate from the Selenium $4s$ atomic orbitals. In the bulk limit, the width of this peak reflects the bandwidth of this narrow low-lying band,[31] which is energetically isolated from all other bands. The states in the range -10 to 0 eV are given by a mixture of the s and p orbitals of both the Se and the Cd atoms. In the bulk these states result in three bands, which have p character, that are situated in this energetic region. In all cases, these lower-lying valence states, which are occupied in the ground state, are separated by a band gap, which increases with decreasing size, from the higher lying (positive energy) states. In the bulk the states above the gap result in six conduction bands. Altogether our 5 orbital per Se and Cd atom model becomes a 10 band model in the bulk limit, including 4 valence and 6 conduction bands. Our results shown in Fig. 1 agree with the calculations of Hill and Whaley.[31] For both the 5-Cd and 5-Se case, we find an energy gap of about 3 eV. We further note that the differences in the density of states of the nanocrystals with a Se or a Cd surface get smaller with increasing size, as the same bulk limit is approached.

To calculate the linear absorption, we assume that initially all the valence states below the gap are filled. We then integrate either Eqs. (2.19) in real-space, or Eq. (B9) in the

TABLE III. The on-site Coulomb interaction energy (D1) of Se and of Cd (in eV).

I^{4s4s}_{Se}	5.945	I^{5s5s}_{Cd}	11.10
$I^{4s4p_x}_{Se}$	5.686	$I^{5s5p_x}_{Cd}$	11.10
$I^{4p_x4p_x}_{Se}$	5.957	$I^{5p_x5p_x}_{Cd}$	11.96
$I^{4p_x4p_y}_{Se}$	5.222	$I^{5p_x5p_y}_{Cd}$	11.73
$I^{4p_x5s}_{Se}$	0.4616	$I^{5p_x6s}_{Cd}$	1.53
I^{4s5s}_{Se}	0.4616	I^{5s6s}_{Cd}	1.53
I^{5s5s}_{Se}	0.3721	I^{6s6s}_{Cd}	1.23

TABLE IV. Non-zero matrix elements of the dipole moment of Se and of Cd (in eÅ).

$\mu^{4s4p_x}_{Se\,x}$	-0.6831	$\mu^{5s5p_x}_{Cd\,x}$	-1.3068
$\mu^{4s4p_y}_{Se\,y}$	-0.6831	$\mu^{5s5p_y}_{Cd\,y}$	-1.3068
$\mu^{4s4p_z}_{Se\,z}$	-0.6831	$\mu^{5s5p_z}_{Cd\,z}$	-1.3068
$\mu^{5s4p_x}_{Se\,x}$	-0.0139	$\mu^{6s5p_x}_{Cd\,x}$	-0.0033
$\mu^{5s4p_y}_{Se\,y}$	-0.0139	$\mu^{6s5p_y}_{Cd\,y}$	-0.0033
$\mu^{5s4p_z}_{Se\,z}$	-0.0139	$\mu^{6s5p_z}_{Cd\,z}$	-0.0033

MO representation in the time domain by applying an ultrashort pulse, polarized along the z-direction (001), and calculated the time evolution of the density matrix. We used a laser pulse with a Gaussian envelope, i.e., $E(t) \propto e^{(-(t/\bar{t})^2)}$, and a duration of $\bar{t}=0.1$ fs. (The spectral width of this ultrashort pulse is about 22 eV.) We included a dephasing time of $T_2=12.5$ fs and propagated in time until typically $6T_2$ after the maximum of the laser pulse, using the fourth order Runge–Kutta method with a time-step of 0.004 fs. After this time most of the optical excitation has decayed. The linear optical spectrum is then obtained by a Fourier transform of the time-dependent polarization

$$P(t)=Tr[\delta\rho(t)\hat{P}]=\sum_{ij\nu\nu'}\mu_{ij}^{\nu\nu'}\delta\rho_{ij}^{\nu\nu'}(t), \tag{3.2}$$

$$P(\omega)=\int_{-\infty}^{\infty}dtP(t)e^{-i\omega t}. \tag{3.3}$$

This gives the complex linear polarizability whose imaginary part $\alpha(\omega)$ is proportional to the absorption lineshape:

$$\alpha(\omega)=\mathrm{Im}[P(\omega)/E(\omega)], \tag{3.4}$$

where $E(\omega)$ is the Fourier transform of the exciting laser pulse.

In Figs. 2, 3, and 4, we display the resulting linear absorption spectra. Figure 2 shows the result for 5-Se. Comparison of the results obtained with and without Coulomb interaction, [calculated solving Eq. (2.19)], demonstrates that in the vicinity of the band gap the excitonic effects lead to a red shift in the absorption spectra and an enhancement of the absorption. The higher lying transitions are also shifted towards lower energies, as shown in the extended scale (bottom panel). Similar trends can be seen in Fig. 3, where the same quantities are displayed for 5-Cd.

The size dependence of the absorption spectra near the band gap is shown in Fig. 4 for 3, 4, and 5 shell nanocrystals with different surfaces. These plots display the increased shift of the absorption lines due to the Coulomb interaction with decreasing size. Within the EMA it was for example predicted that the exciton binding energy should scale like $1/R$, where R is the radius of the nanocrystal. The EMA fails to reproduce the experimentally observed absorption spectra for small sizes.[32] The weak absorption peaks appearing below the main absorption line result from the Coulomb exchange interaction, which leads to almost dark excitons situated energetically below the main transition.[12,20,52,53] These features disappear when the exchange term is neglected. Although the nanocrystals investigated here are too small to compare directly with experiment, this result seems to reinforce the idea that the lowest state is nearly forbidden and that the luminescence should therefore be long lived.[12]

In the following we analyze the size dependence of the lowest absorption feature and of the exciton binding energy and compare them with results of the EMA and with experiment. Figure 5 shows the lowest strong peak (indicated by a * in Fig. 4) as a function of the nanocrystal diameter. Without Coulomb interaction [dotted line (A) in Fig. 5]) the band gap is too high. Using the diagonal approximation within the MO basis, retaining only the attractive Hartree-term [Eq. (B11)], the energy of the lowest absorption feature decreases.[32] This effect is shown as a dashed-dotted line (B). The inclusion of the Fock term [Eq. (B10)], which represents a repulsive potential between electrons and holes, increases the exciton energy [see long-dashed line (C)]. As expected, the importance of the Fock term increases with decreasing system size, since this term is negligible for bulk semiconductors.[46,54] Previous calculations have neglected this term also for nanocrystals.[32] However, for the small nanocrystals studied in this paper this term may not be neglected.

To obtain lower exciton energies, and a better agreement with experiment,[32] one needs to include also the off-diagonal terms of the Coulomb interaction [Eq. (B9) and (2.19)]. As shown in Fig. 5 (curve D), these off-diagonal terms reduce the exciton energies even below the values obtained in the diagonal Hartree approximation. (For the Se surface case the exciton energy including the contribution of the off-diagonal terms comes at even higher energy than the case with the diagonal Hartree–Fock exciton energy. However there is no inconsistency here. In the case of the calculation including the off-diagonal terms there are some absorption peaks in the energy region which is lower than the lowest strong peak as in Fig. 4.) Within the calculation which includes the off-diagonal terms, the resulting excitons can be viewed as real collective excitations, because all the electron-hole components of the density matrix are coupled. All of these conclusions are consistent with Fig. 6, which shows the exciton binding energies for the same approximations shown in Fig. 5. To obtain these values we computed the absorption spectra for different models. The binding energy is then given by the difference between the spectral position of the exciton compared to calculation (A) in Fig. 5, where the Coulomb interaction has been neglected.

In Fig. 7 we compare our values for the size-dependent exciton energies with previous calculations[24,32] and with experiment. The EMA results in too high exciton energies, and our results are much closer to the experiment. Here we compare the lowest strong absorption peak of the Cd surface nanocrystal with experiment. This is because the difference of the surface of the nanocrystal is not distinguished in the experiment of the absorption. Then it turns out that the avarage for the Cd and Se surface case should be taken to compare the experimental results. The lowest strong absorption peak of the Cd surface case shows the lower energy than the Se surface case, so that this peak become the lowest strong peak when the avarage of absorption spectrum of the Cd and Se surface case is taken. By including off-diagonal Coulomb-matrix elements, we obtained larger exciton binding energies (and therefore lower exciton energies), compared to previous TB methods,[32] in better agreement with experiment.

The electronic density matrix allows a direct real-space interpretation of optical excitations. The eigenmodes of the linear TDHF equations constitute a set of electron-hole oscillators. The dynamics of electronic excitations is thus

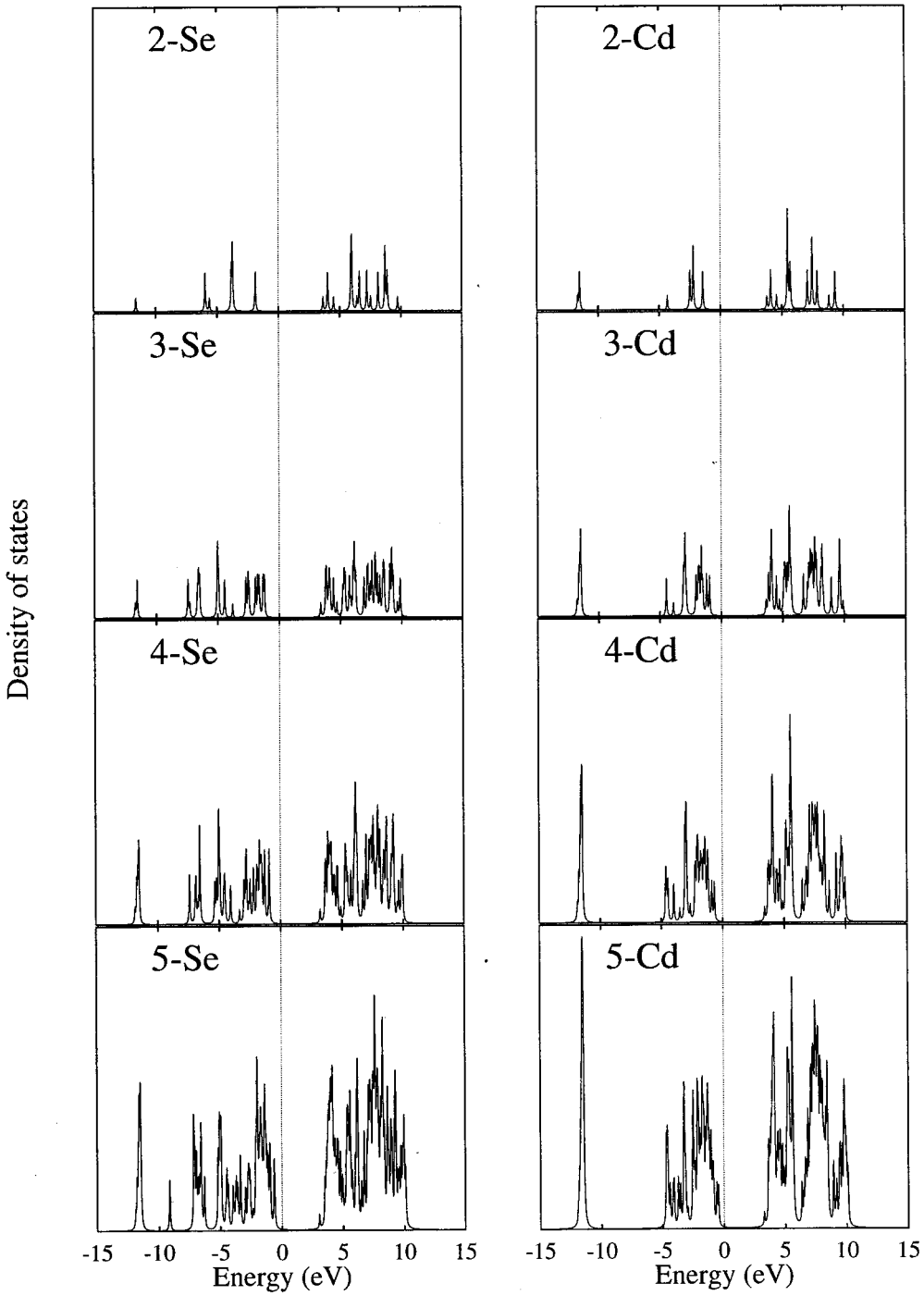

FIG. 1. Density of states for various nanocrystal sizes with Se surfaces (left) and Cd surfaces (right).

mapped onto a set of coupled real space oscillators and the optical response may be interpreted without alluding to specific eigenstates. For linear polyenes, contour plots of the density matrix show the charges and the electronic coherences induced by the electric field at a given frequency. To apply the same analysis we introduce the electronic coherence matrix between atom i and an atom j

$$c_{i,j}=(1-\delta_{ij})\sqrt{\sum_{\nu_1\nu_2}|\delta\rho_{ij}^{\nu_1\nu_2}(\omega)|^2}, \tag{3.5}$$

where $\delta\rho_{ij}^{\nu_1\nu_2}(\omega)$ is obtained by the Fourier cosine transfor-

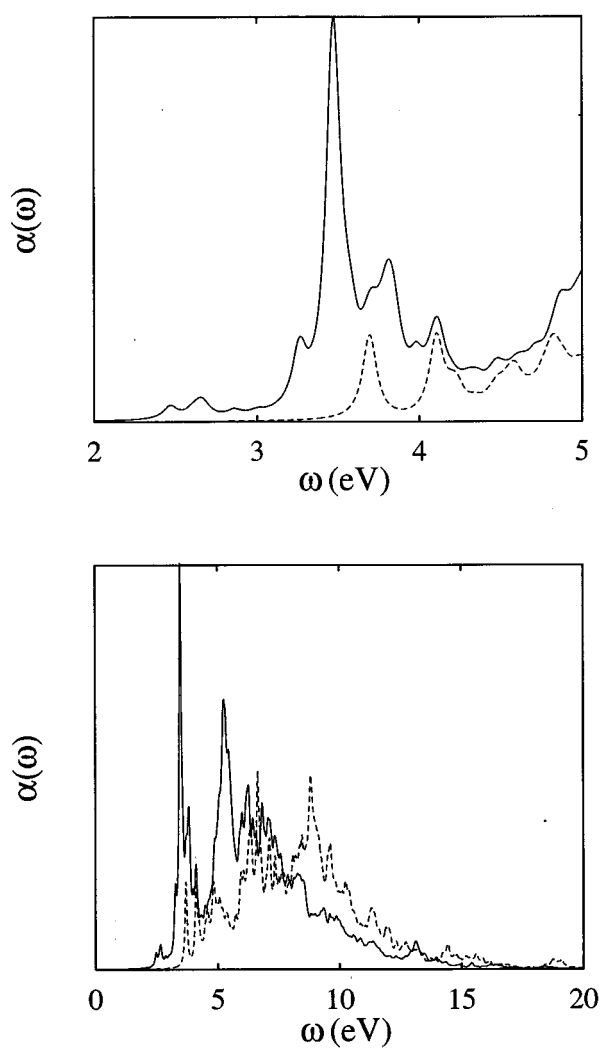

FIG. 2. Absorption spectra $\alpha(\omega)$ for a 5-Se nanocrystal with (solid line) and without (dashed line) Coulomb interaction. Top panel in the vicinity of the band edge and bottom panel over the entire spectral range covered by our model.

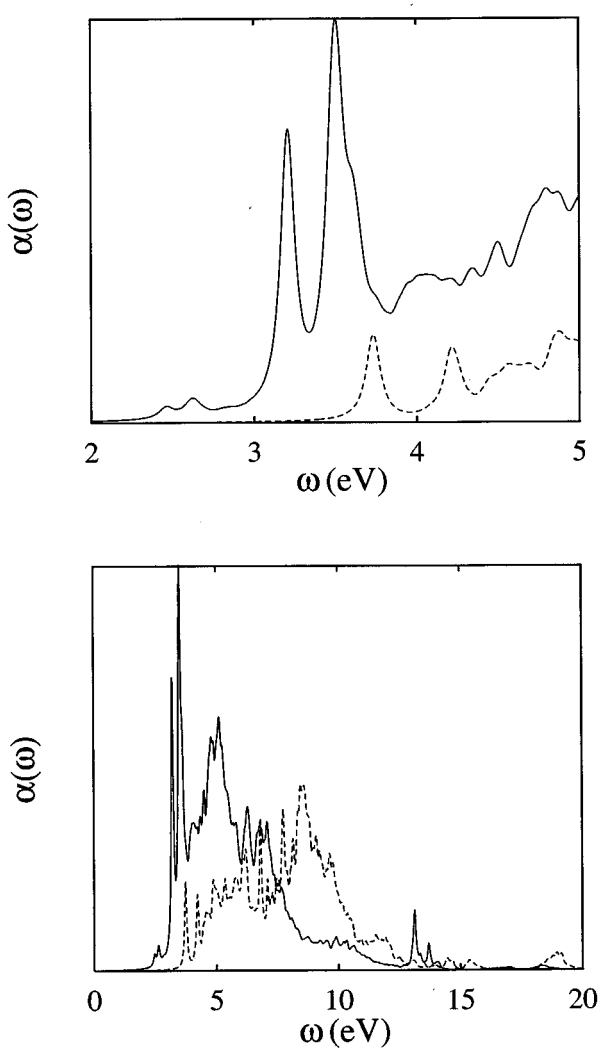

FIG. 3. Same as Fig. 2 but for 5-Cd.

mation of $\delta\rho_{ij}^{\nu_1\nu_2}(t)$. This represents the off-diagonal density matrix between two atoms, averaged over the various orbitals.

The electronic coherence matrix for the ground state and in the lowest-lying excited states along the (011) direction and the (110) direction for 3-, 4-, and 5-Cd are shown in Fig. 8. [Calculations made along the (101) and (-101) directions are exactly the same as the (011) calculations. Calculations for the Se surface are also very similar. These are not shown.]

Figures 8(a)–8(c) shows that the ground state correlations [obtained by replacing $\delta\rho$ with $\overline{\rho}$ in Eq. (3.5)] are of very short range. Only electrons on nearest neighbor and next-nearest neighbor atoms are correlated, i.e. have any coherence. However, for the excited states these electronic coherences extend over a much larger range. The extent of these coherences is for these sizes of the nanocrystals mainly determined by the physical size of the nanocrystal. Figs. 8(d)–8(i) therefore illustrates how the optical excitation induces electronic coherence in the system. This is very similar to the behavior in conjugated polyenes.[41] Since the correlation are similar in both directions, we can conclude that the excitons are spherical. Furthermore the large values of the coherences around the central atom indicates that the lowest exciton is mainly concentrated near the nanocrystal center. Had this been a surface state, the correlation matrix would look completely different; the largest values would be in the outer shells. For large nanocrystals we approach the bulk limit, and the lowest excitation evolves into the Wannier-exciton. The electronic correlation of the Wannier-exciton, which is a hydrogenic $1s$ wavefunction for the relative coordinate with a Bohr radius of 55.9 Å for CdSe and has no dependence on the center-of-mass coordinate,[46] is shown in Fig. 9(b). For large nanocrystals with radius comparable or larger than the Bohr radius of the bulk exciton (which corresponds to 30 shells or more) the intrinsic coherence length, which can be determined from Fig. 8 by the spread of the

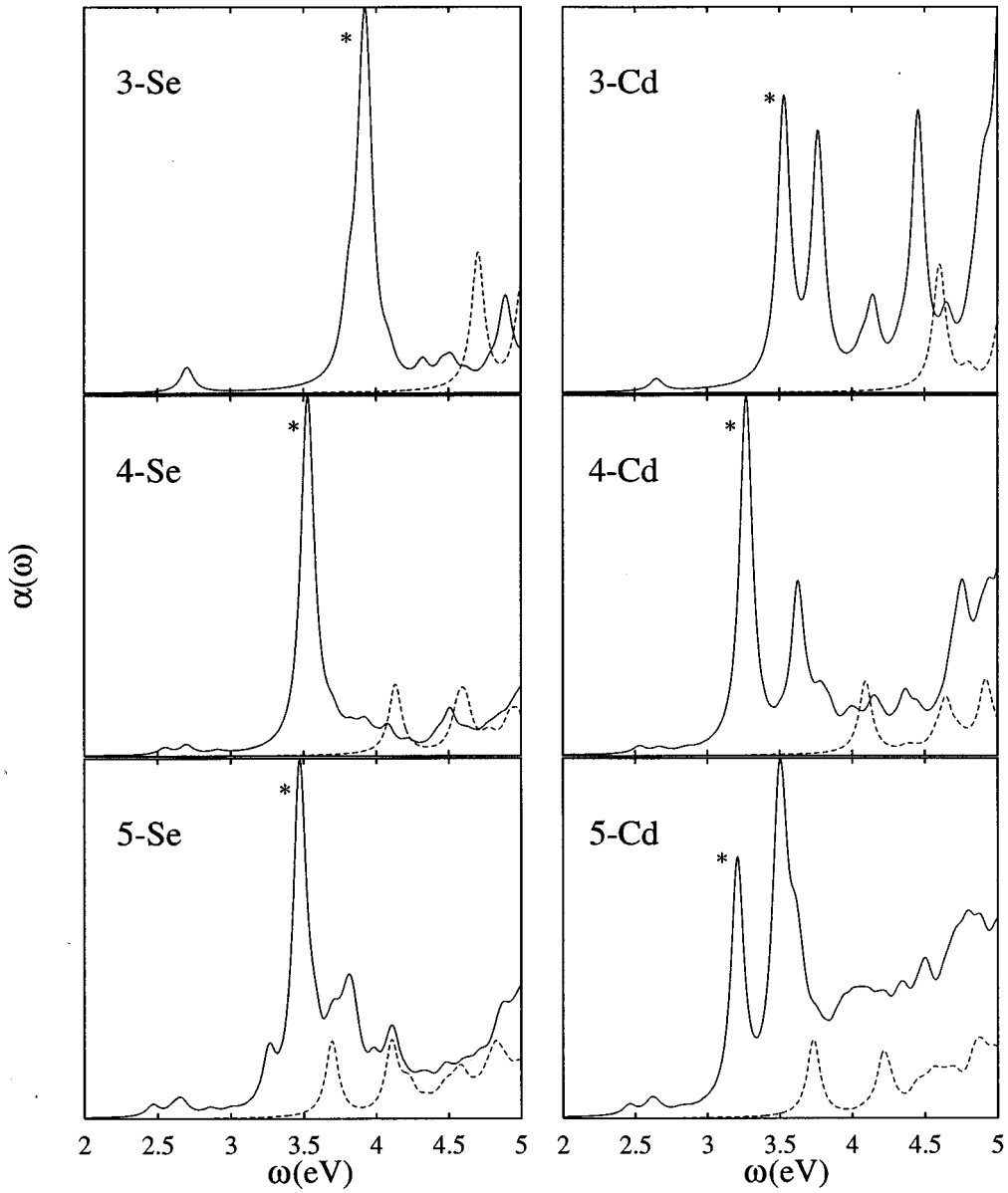

FIG. 4. Absorption spectra in the vicinity of the band gap calculated with (solid line) and without (dashed line) Coulomb interaction for various nanocrystals, as indicated. Asterisks in the figure represent the lowest strong absorption peaks.

coherence matrix along the ''antidiagonal'' direction, no longer coincides with the nanocrystal size, but will saturate and approach the exciton Bohr radius.

Figure 9 shows the coherence matrices of the ground state, the almost dark (exchange split-off) exciton, and main exciton for 3-Se. Both transitions are concentrated around the center of the nanocrystal. This again confirms our interpretation of the appearance of the transitions with small oscillator strength and proves that these are not surface states. Figure 10 shows the densities of the ground and the excited states corresponding to the main and the exchange split-off excitons, which are given by

$$n_i = \sum_{\nu} \delta\rho_{ii}^{\nu\nu}. \tag{3.6}$$

In the ground state in all directions the charge density is symmetric with respect to the center of the nanocrystal. For the excited states the charge density is still symmetric in the (110) direction which is perpendicular to the polarization (z) direction of the exciting electric field. For the (011) direction, which involves the z direction, the charge density is anti-symmetric due to the dipole coupling to the external field.

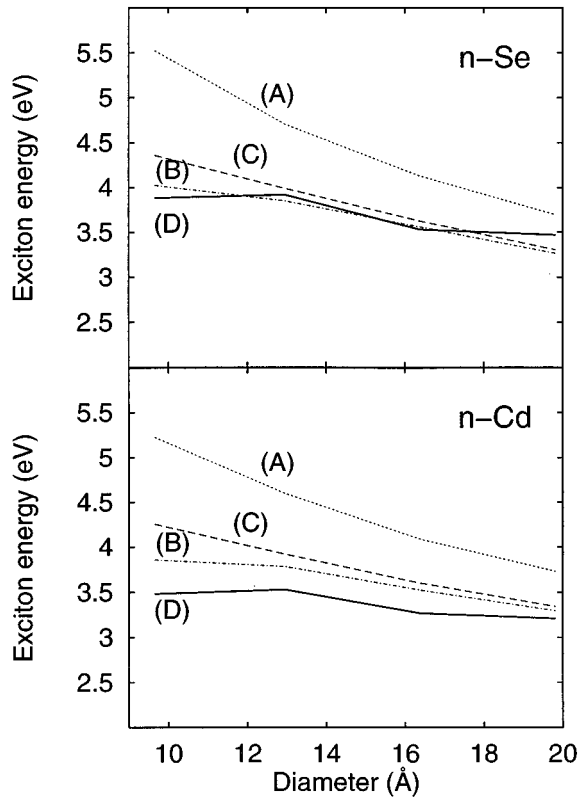

FIG. 5. Energies of the energetically lowest exciton with large oscillator strength for the Se and Cd surface case for different approximations: (A) neglecting the Coulomb-interaction (dotted), (B) diagonal approximation for Coulomb matrix elements keeping only the Hartree-term (dashed-dotted), (C) diagonal approximation keeping Hartree and Fock-terms (long-dashed), and (D) full calculation including all Coulomb matrix elements (solid). In the case of full calculation, we plot the exciton energy of the lowest strong peak which is indicated by asterisk in Fig. 4.

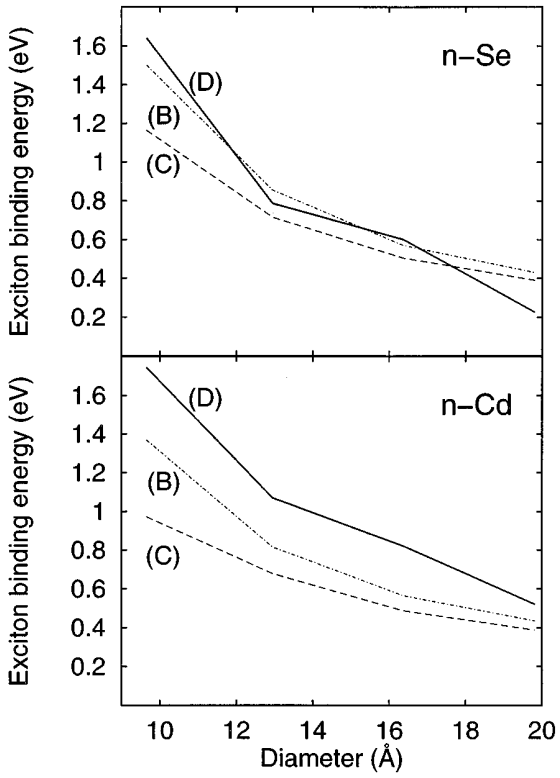

FIG. 6. Binding energies of the energetically lowest exciton with large oscillator strength for the Se and the Cd surface case using approximations (B), (C), and (D) of Fig. 5.

IV. DISCUSSION

The size dependence of the absorption spectra of semiconductor nanocrystals was analyzed using the equations of motion for the reduced single-electron density matrix. The equations are derived starting with a tight-binding Hamiltonian which systematically includes the Coulomb interaction. We discussed the influence of the different types of Coulomb interactions and showed that Fock-type interaction, which is negligible for large systems, needs to be included in small systems. This interaction leads to almost dark excitons, which show up below the main exciton transition. The inclusion of off-diagonal Coulomb-matrix elements results in a collective nature of the optical excitation, and leads to larger exciton binding energies and a better agreement with experimental transition energies compared with previous theoretical studies. A clear connection has been established between the interatomic electronic coherence (off-diagonal elements of the density matrix) and the optical spectra. For example, we have shown that both the weak below gap transitions as well as the main exciton are concentrated around the center of the nanocrystal and are not surface states. The present approach provides a unified treatment of the optical response of semiconductor nanostructures, conjugated polyenes, and molecular aggregates. In future studies it should be possible to investigate also nonlinear optical signals, such as four-wave mixing, photon echo and hole-burning[8,13] using the equations presented in this paper. The required numerical effort is not considerably larger than the calculations of the linear response presented here. Additionally the present ap-

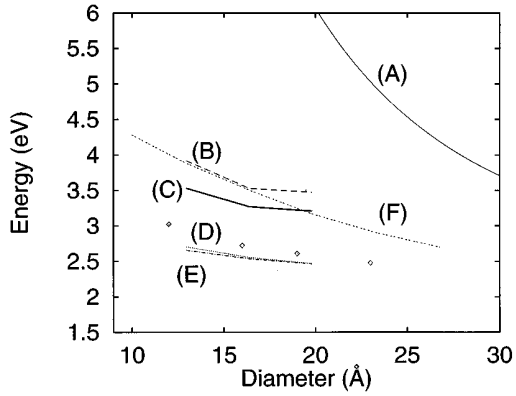

FIG. 7. Exciton energies for different models. (A) effective mass model (solid), energies of the energetically lowest exciton with large oscillator strength (B) for the Se (long-dashed), and (C) for the Cd (thick-solid) surface case, energies of the energetically lowest excitons, which do not show large absorption (D) for the Se (dotted), and (E) for the Cd (dashed-dotted) surface case (F) (double-dashed) the results of Ref. 32. Experimental results (diamonds) are taken from Ref. 6.

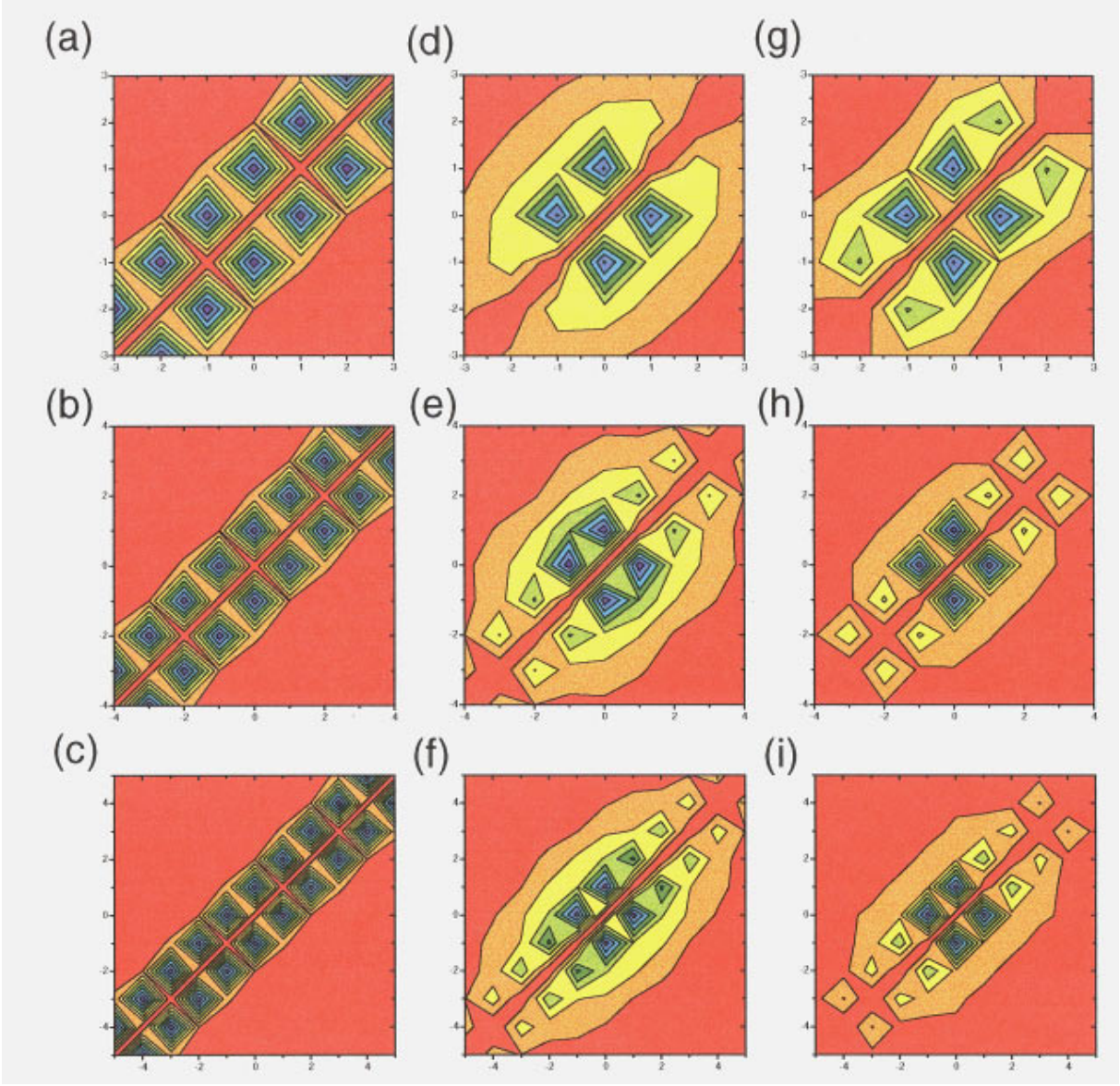

FIG. 8. The electronic coherence matrix showing correlations between electrons on different atoms. The systems shown from top to bottom are 3-Cd, 4-Cd, and 5-Cd. Left column: the ground state. Middle column: at (d) $\omega=2.66$(eV), (e) $\omega=2.53$(eV), and (f) $\omega=2.44$(eV) corresponding to the energetically lowest excited state along (011). Right column: at (g) $\omega=2.70$(eV), (h) $\omega=2.55$(eV), (i) $\omega=2.44$(eV) corresponding to the energetically lowest excited state along (110). The Wannier-exciton in CdSe, which is reached in the bulk-limit is shown on Fig. 9(b). [Large=blue (corresponding to 87.6%–100% of the maximum value), green, yellow, red=small (0%–12.5%).]

proach may be used to study much larger systems. Although the ordinary TDHF approach cannot be applied for large nanocrystals because of computational limitations, it should be possible to apply the density matrix spectral moment algorithm,[57] which has been successfully used to calculate optical spectra of large conjugated polyene chains with a few hundred carbon atoms. This should make it possible to study much larger nanocrystals, and provide a microscopic theory which can be used to study the evolution of bulk properties with size.

ACKNOWLEDGMENTS

We acknowledge helpful discussions with N. A. Hill and K. B. Whaley regarding their calculations. The support of the Air Force office of scientific research, and the NSF through Grants No. CHE-9526125 and No. PHY94-15583 is gratefully acknowledged. T. M. acknowledges financial support by a fellowship from the scientific branch of the NATO through the Deutscher Akademischer Austauschdienst (DAAD).

APPENDIX A: HIGHER ORDER EQUATIONS FOR THE DENSITY MATRIX IN REAL-SPACE

We have expressed the optical response in real space using matrix notation, see Eq. (2.17). In this Appendix we develop a scheme for calculating the optical response to all

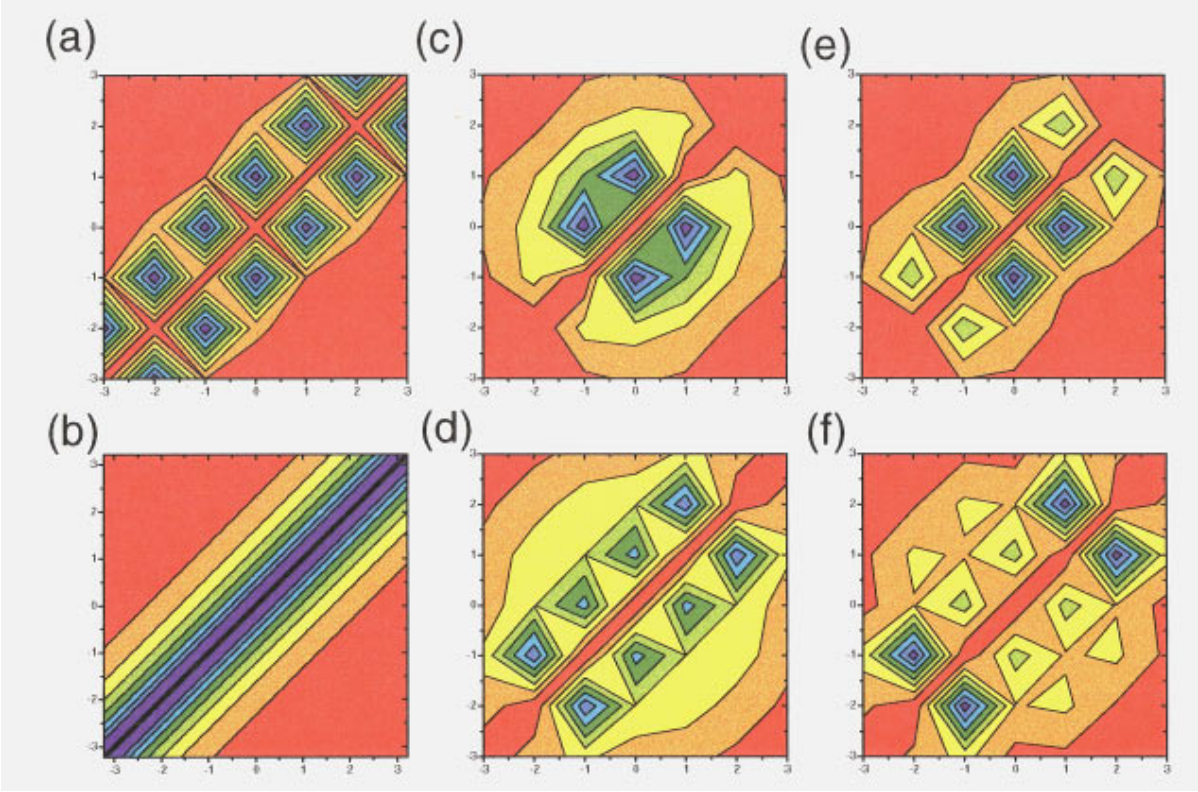

FIG. 9. The coherence matrix showing correlations between electrons on different atoms for the first and second excited state for 3-Se case is shown along (011) (middle column), and along (110) (right hand side column). The first and second row correspond to the first and second excited state for 3-Se. The ground state correlation matrix for 3-Se is also shown on (a). The Wannier-exciton in CdSe, which is reached in the bulk-limit is shown on (b) (here the distance is measured in units of the Bohr radius). [Large=blue (corresponding to 87.6[%]–100% of the maximum value), green, yellow, red=small (0%–12.5%).]

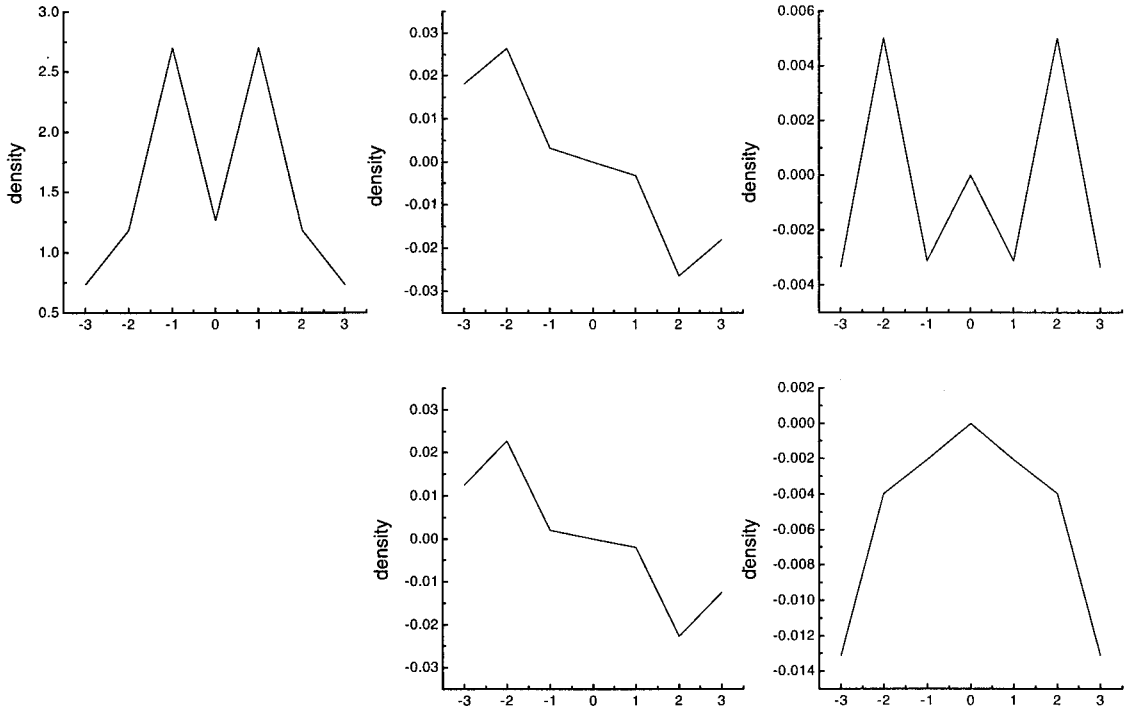

FIG. 10. The densities for the first and second excited states for 3-Se case is shown along (110) (right hand side column), and along (011) (middle column). The density for the ground state for 3-Se is also shown (left hand side column). For the excited state part, the first and second row correspond to the first and second excited state for 3-Se.

orders in the field, and give the necessary equations of motions for the density matrix. In the following spin indices are included in the site indices in real space.

In order to study the nonliner response, we need to expand $\delta\rho$ in the external field,

$$\delta\rho=\sum_{k=1}^{\infty}\delta\rho^{(k)} \tag{A1}$$

where $\rho^{(k)}$ is the k-th order term. Inserting (A1) into (2.17), we obtain the k-th order ($k\geqslant 2$):

$$i\hbar\frac{d}{dt}\delta\rho^{(k)}=[h(\overline{\rho}),\delta\rho^{(k)}]+[\delta h(\delta\rho^{(k)}),\overline{\rho}] +[f,\delta\rho^{(k-1)}]+\sum_{l=1}^{k-1}[\delta h(\delta\rho^{(l)}),\delta\rho^{(k-l)}]. \tag{A2}$$

Here $\delta h(\delta\rho^{(k)})$ is given by

$$\begin{aligned}\delta h_{ji}^{\nu'\nu}(\delta\rho^{(k)})=&+\frac{1}{2}\delta_{ji}\sum_{i_2\nu_3\nu_4}V_1\binom{\nu'\nu\nu_3\nu_4}{ii_2}\delta\rho_{i_2i_2}^{(k)\nu_4\nu_3}\\&-\frac{1}{2}\sum_{\nu_2\nu_3}V_1\binom{\nu'\nu_2\nu_3\nu}{ji}\delta\rho_{ji}^{(k)\nu_2\nu_3}\\&-\frac{1}{2}\sum_{\nu_1\nu_4}V_1\binom{\nu_1\nu\nu'\nu_4}{ij}\delta\rho_{ji}^{(k)\nu_4\nu_1}\\&+\frac{1}{2}\delta_{ji}\sum_{i_1\nu_1\nu_2}V_1\binom{\nu_1\nu_2\nu'\nu}{i_1i}\delta\rho_{i_1i_1}^{(k)\nu_2\nu_1}.\end{aligned} \tag{A3}$$

Equations (A2) and (A3) can be used to iteratively calculate the optical response order by order.

APPENDIX B: EQUATIONS OF MOTION IN THE MOLECULAR-ORBITAL REPRESENTATION

To transform Eqs. (2.18) and (A2) to the molecular orbital basis set, we start by determining the ground state of the nanocrystal. A diagonalization of the Fock matrices of the ground state, $h_{ji}^{\nu'\nu}(\overline{\rho})$, determines the molecular orbitals (MO) and the density of states of the nanocrystal. In the MO basis we can distinguish between electrons (p) and holes (h), corresponding to MOs with energies above (below) the band gap which are unoccupied (occupies) in the ground state.

We next transform the Hamiltonian from real-space to the MO basis:

$$\hat{H}_0=\sum_{e_1,e_2=p,h}T^{e_1e_2}\hat{c}_{e_1}^{\dagger}\hat{c}_{e_2}. \tag{B1}$$

Here $\hat{c}_{h_1}^{\dagger}$ ($\hat{c}_{p_1}^{\dagger}$) and $\hat{c}_{h_1}$ ($\hat{c}_{p_1}$) are the creation and annihilation operators corresponding to occupied (unoccupied) MOs and e stands for both occupied (h) and unoccupied (p) MOs. The interaction Hamiltonian is:

$$\hat{H}_{\rm int}=-\vec{E}(t)\cdot\Bigg[\sum_{h_1h_2}\vec{\mu}^{h_1h_2}\hat{c}_{h_1}^{\dagger}\hat{c}_{h_2}+\sum_{p_1p_2}\vec{\mu}^{p_1p_2}\hat{c}_{p_1}^{\dagger}\hat{c}_{p_2} +\sum_{h_1p_1}(\vec{\mu}^{h_1p_1}\hat{c}_{h_1}^{\dagger}\hat{c}_{p_1}+\vec{\mu}^{p_1h_1}\hat{c}_{p_1}^{\dagger}\hat{c}_{h_1}). \tag{B2}$$

The Coulomb interaction can be written as:

$$\hat{H}_c=\frac{1}{2}\sum_{e_1,e_2,e_3,e_4=p,h}V_1(e_1e_2e_3e_4)\hat{c}_{e_1}^{\dagger}\hat{c}_{e_3}^{\dagger}\hat{c}_{e_4}\hat{c}_{e_2}, \tag{B3}$$

The TDHF equations of motion then assume the following form:

$$\begin{aligned}i\hbar\frac{d}{dt}\delta\rho_{e'e}=&(h_{e'e'}(\overline{\rho})-h_{ee}(\overline{\rho}))\delta\rho_{e'e}+\vec{E}(t)\cdot\Bigg(\sum_{e_1}\vec{\mu}_{e_1e}\overline{\rho_{e'e_1}}-\sum_{e_2}\vec{\mu}_{e'e_2}\overline{\rho_{e_2e}}\Bigg)+\vec{E}(t)\cdot\Bigg(\sum_{e_1}\vec{\mu}_{e_1e}\delta\rho_{e'e_1}-\sum_{e_2}\vec{\mu}_{e'e_2}\delta\rho_{e_2e}\Bigg)\\&+\sum_{e_1e_2e_3}\frac{1}{2}V_1(e_1e_2e_3e)(\delta\rho_{e_2e_3}\overline{\rho_{e'e_1}}-2\delta\rho_{e_2e_1}\overline{\rho_{e'e_3}}+\delta\rho_{e_2e_3}\delta\rho_{e'e_1}-2\delta\rho_{e_2e_1}\delta\rho_{e'e_3})-\sum_{e_1e_3e_4}\frac{1}{2}V_1(e_1ee_3e_4)\\&\times(2\delta\rho_{e_4e_3}\overline{\rho_{e'e_1}}-\delta\rho_{e_4e_1}\overline{\rho_{e'e_3}}+2\delta\rho_{e_4e_3}\delta\rho_{e'e_1}-\delta\rho_{e_4e_1}\delta\rho_{e'e_3})+\sum_{e_2e_3e_4}\frac{1}{2}V_1(e'e_2e_3e_4)(2\delta\rho_{e_4e_3}\overline{\rho_{e_2e}}\\&-\overline{\rho_{e_4e}}\delta\rho_{e_2e_3}+2\delta\rho_{e_4e_3}\delta\rho_{e_2e}-\delta\rho_{e_4e}\delta\rho_{e_2e_3})-\sum_{e_1e_2e_4}\frac{1}{2}V_1(e_1e_2e'e_4)(\delta\rho_{e_4e_1}\overline{\rho_{e_2e}}-2\overline{\rho_{e_4e}}\delta\rho_{e_2e_1}+\delta\rho_{e_4e_1}\delta\rho_{e_2e}\\&-2\delta\rho_{e_4e}\delta\rho_{e_2e_1}),\end{aligned} \tag{B4}$$

where

$$\rho_{e_1e_2}(t)=\langle\Psi(t)|\hat{\rho}_{e_1e_2}|\Psi(t)\rangle. \tag{B5}$$

Here e_i may correspond to either an occupied (h_i) or an unoccupied (p_i) MO, and $\overline{\rho_{e_1e_2}}$ is the ground state density matrix. We have summed over the spin indices and no additional summations over spin are needed in (B5) and in the following. In the MO basis, the ground state density matrix is diagonal and only nonvanishing if $e_1=e_2=h_i$ for some occupied MO. Equation (B4) can be used to analyze the optical response to all orders in the external field; application to the nonlinear response is discussed in Appendix C. In the following we develop and discuss the equations for the linear response.

The equation of motion for the electron-hole part of the density matrix $\delta\rho_{ph}$ reads

$$
\begin{aligned}
i\hbar\frac{d}{dt}\delta\rho_{ph} &= (h_{pp}(\overline{\rho})-h_{hh}(\overline{\rho}))\,\delta\rho_{ph}-\vec{E}(t)\cdot\vec{\mu}_{ph}+\sum_{p_1}\vec{E}(t)\cdot(\vec{\mu}_{p_1h}\delta\rho_{pp_1}-\vec{\mu}_{pp_1}\delta\rho_{p_1h})+\sum_{h_1}\vec{E}(t)\cdot(\vec{\mu}_{h_1h}\delta\rho_{ph_1}\\
&-\vec{\mu}_{ph_1}\delta\rho_{h_1h})+\sum_{p_1p_2}V_2(php_1p_2)\,\delta\rho_{p_1p_2}+\sum_{h_1h_2}V_2(phh_1h_2)\,\delta\rho_{h_1h_2}+\sum_{p_1h_1}(V_1(php_1h_1)\,\delta\rho_{h_1p_1}\\
&+V_1(phh_1p_1)\,\delta\rho_{p_1h_1})-\frac{1}{2}\sum_{p_1h_1}(V_1(pp_1h_1h)\,\delta\rho_{p_1h_1}+V_1(ph_1p_1h)\,\delta\rho_{h_1p_1})-\frac{1}{2}\sum_{p_1h_1}(V_1(p_1hph_1)\,\delta\rho_{h_1p_1}\\
&+V_1(h_1hpp_1)\,\delta\rho_{p_1h_1})+\sum_{p_1h_1}(V_1(p_1h_1ph)\,\delta\rho_{h_1p_1}+V_1(h_1p_1ph)\,\delta\rho_{p_1h_1})+\sum_{e_1e_2e_3}\frac{1}{2}V_1(e_1e_2e_3h)(\delta\rho_{e_2e_3}\delta\rho_{pe_1}\\
&-2\,\delta\rho_{e_2e_1}\delta\rho_{pe_3})-\sum_{e_1e_3e_4}\frac{1}{2}V_1(e_1he_3e_4)(2\,\delta\rho_{e_4e_3}\delta\rho_{pe_1}-\delta\rho_{e_4e_1}\delta\rho_{pe_3})+\sum_{e_2e_3e_4}\frac{1}{2}V_1(pe_2e_3e_4)(2\,\delta\rho_{e_4e_3}\delta\rho_{e_2h}\\
&-\delta\rho_{e_4h}\delta\rho_{e_2e_3})-\sum_{e_1e_2e_4}\frac{1}{2}V_1(e_1e_2pe_4)(\delta\rho_{e_4e_1}\delta\rho_{e_2h}-2\,\delta\rho_{e_4h}\delta\rho_{e_2e_1}),
\end{aligned}
\tag{B6}
$$

where V_2 is given by

$$
V_2(phe_1e_2)=V_1(phe_2e_1)-\frac{1}{2}V_1(pe_1e_2h)-\frac{1}{2}V_1(e_2hpe_1)+V_1(e_2e_1ph). \tag{B7}
$$

For calculating the linear response, we only need the electron-hole part of the density matrix. [From (B4), it is easy to verify that the equations of motion of the hole–hole part and electron–electron parts of the density matrix are at least of second order in the external field.]

$$
\begin{aligned}
i\hbar\frac{d}{dt}\delta\rho_{ph}(t) &= (h_{pp}(\overline{\rho})-h_{hh}(\overline{\rho}))\,\delta\rho_{ph}-\vec{E}(t)\cdot\vec{\mu}_{ph}+\sum_{p_1h_1}\Big[V_1(php_1h_1)-\frac{1}{2}V_1(ph_1p_1h)-\frac{1}{2}V_1(p_1hph_1)\\
&+V_1(p_1h_1ph)\Big]\delta\rho_{h_1p_1}+\sum_{p_1h_1}\Big[V_1(phh_1p_1)-\frac{1}{2}V_1(pp_1h_1h)-\frac{1}{2}V_1(h_1hpp_1)+V_1(h_1p_1ph)\Big]\delta\rho_{p_1h_1}.
\end{aligned}
\tag{B8}
$$

Using the relation $\rho_{hp}=\rho_{ph}^{\dagger}$ we can solve (B8). However the contribution of the first sum on the right hand side of (B8) is negligible, because the frequencies of $\delta\rho_{h_1p_1}$ and $\delta\rho_{p_1h_1}$ have opposite sign (the rotating-wave approximation). We thus have

$$
\begin{aligned}
i\hbar\frac{d}{dt}\delta\rho_{ph}(t) &= (h_{pp}(\overline{\rho})-h_{hh}(\overline{\rho}))\,\delta\rho_{ph}-\vec{E}(t)\cdot\vec{\mu}_{ph}\\
&+\sum_{p_1h_1}\Big(V_1(phh_1p_1)-\frac{1}{2}V_1(pp_1h_1h)\\
&-\frac{1}{2}V_1(h_1hpp_1)+V_1(h_1p_1ph)\Big)\delta\rho_{p_1h_1}.
\end{aligned}
\tag{B9}
$$

Equation (B9) determines the electron-hole part of the density matrix, which completely determines the linear optical response. The first term $[h_{pp}(\overline{\rho})-h_{hh}(\overline{\rho})]\delta\rho_{ph}$ results in a rotation with a frequency given by the energy difference between the electron and hole states. The second term is the dipole coupling to the external field, which is proportional to the dipole matrix element $\vec{\mu}_{ph}$. The other terms describe Coulomb interactions between electrons and holes. Note that due to the summations over p_1 and h_1, all the electron-hole components are coupled, which gives rise to collective resonances, appearing as excitons. The attractive Hartree terms ($V_1(pp_1h_1h)$ and $V_1(h_1hpp_1)$) are dominant in bulk semiconductors,[46,48,49] the repulsive Fock terms [$V_1(phh_1p_1)$ and $V_1(h_1p_1ph)$], however, become increasingly important for small systems. A quantitative evaluation of the individual contributions of the different Coulomb terms is given in Sec. III.

In addition to the complete solution of Eqs. (B8), we have examined some simplified approximations. If we only retain the diagonal part of the Coulomb interaction in the

MO, [neglecting the summations over p_1 and h_1 in Eq. (B9)] the equation is simplified considerably:

$$i\hbar\frac{d}{dt}\delta\rho_{ph}(t)=(h_{pp}(\overline{\rho})-h_{hh}(\overline{\rho}))\delta\rho_{ph}-\vec{E}(t)\cdot\vec{\mu}_{ph}+\frac{1}{2}(2V_1(phhp)-V_1(pphh)-V_1(hhpp)+2V_1(hpph))\delta\rho_{ph}. \tag{B10}$$

This equation includes the Hartree and Fock Coulomb interaction of each individual electron-hole component of the density matrix. Since the coupling between different transitions is neglected, the excitons are no longer real collective excitations of the system. By inspection of the equation one finds that within this approximation the Coulomb interaction simply results in an energy shift of the individual transition energies.

Another simplification would be to completely neglect the Fock part of the Coulomb interaction, which is commonly done for large systems. This results in:

$$i\hbar\frac{d}{dt}\delta\rho_{ph}(t)=(h_{pp}(\overline{\rho})-h_{hh}(\overline{\rho}))\delta\rho_{ph}-\vec{E}(t)\cdot\vec{\mu}_{ph}-\frac{1}{2}(V_1(pphh)+V_1(hhpp))\delta\rho_{ph}. \tag{B11}$$

A discussion of these two approximations is given in Sec. III, where we show that the Fock term, which reduces the exciton binding energy, becomes increasingly important with decreasing system size.

APPENDIX C: HIGHER ORDER EQUATIONS OF MOTION IN THE MOLECULAR-ORBITAL REPRESENTATION

In the MO representation, higher orders of the equations of motion are given by the combination of (B6) and the electron–electron and hole–hole parts of the equations of motion (B4). However, in the TDHF scheme, we need not solve the equations of motion for the electron–electron and hole–hole parts of the density matrix.[37,40] Since the density matrix satisfies $\rho^2(t)=\rho(t)$, substituting $\rho(t)=\overline{\rho}+\delta\rho(t)$, and using $\overline{\rho_{hh'}}=\delta_{hh'}$ and $\overline{\rho_{pp'}}=0$ which results from the solutions of the HF equation, we obtain

$$\delta\rho_{hh'}(t)=-\sum_e \delta\rho_{he}(t)\delta\rho_{eh'}(t), \tag{C1}$$

$$\delta\rho_{pp'}(t)=\sum_e \delta\rho_{pe}(t)\delta\rho_{ep'}(t). \tag{C2}$$

We can use Eqs. (B6), (C1), and (C2) to solve the nonlinear response. The k-th order equations ($k\geqslant 2$) is

$$\begin{aligned}
i\hbar\frac{d}{dt}\delta\rho_{ph}^{(k)}=&(h_{pp}(\overline{\rho})-h_{hh}(\overline{\rho}))\delta\rho_{ph}^{(k)}+\sum_{p_1}\vec{E}(t)\cdot(\vec{\mu}_{p_1h}\delta\rho_{pp_1}^{(k-1)}-\vec{\mu}_{pp_1}\delta\rho_{p_1h}^{(k-1)})+\sum_{h_1}\vec{E}(t)\cdot(\vec{\mu}_{h_1h}\delta\rho_{ph_1}^{(k-1)}-\vec{\mu}_{ph_1}\delta\rho_{h_1h}^{(k-1)})\\
&+\sum_{p_1p_2}V_2(php_1p_2)\delta\rho_{p_1p_2}^{(k)}+\sum_{h_1h_2}V_2(phh_1h_2)\delta\rho_{h_1h_2}^{(k)}+\sum_{p_1h_1}(V_2(phh_1p_1)\delta\rho_{h_1p_1}^{(k)}+V_2(php_1h_1)\delta\rho_{p_1h_1}^{(k)})\\
&+\sum_{e_1e_2e_3}\sum_{l=1}^{k-1}\frac{1}{2}V_1(e_1e_2e_3h)(\delta\rho_{e_2e_3}^{(l)}\delta\rho_{pe_1}^{(k-l)}-2\delta\rho_{e_2e_1}^{(l)}\delta\rho_{pe_3}^{(k-l)})-\sum_{e_1e_3e_4}\sum_{l=1}^{k-1}\frac{1}{2}V_1(e_1he_3e_4)(2\delta\rho_{e_4e_3}^{(l)}\delta\rho_{pe_1}^{(k-l)}\\
&-\delta\rho_{e_4e_1}^{(l)}\delta\rho_{pe_3}^{(k-l)})+\sum_{e_2e_3e_4}\sum_{l=1}^{k-1}\frac{1}{2}V_1(pe_2e_3e_4)(2\delta\rho_{e_4e_3}^{(l)}\delta\rho_{e_2h}^{(k-l)}-\delta\rho_{e_4h}^{(l)}\delta\rho_{e_2e_3}^{(k-l)})-\sum_{e_1e_2e_4}\sum_{l=1}^{k-1}\frac{1}{2}V_1(e_1e_2pe_4)\\
&\times(\delta\rho_{e_4e_1}^{(l)}\delta\rho_{e_2h}^{(k-l)}-2\delta\rho_{e_4h}^{(l)}\delta\rho_{e_2e_1}^{(k-l)}),
\end{aligned} \tag{C3}$$

$$\delta\rho_{hh'}^{(k)}(t)=-\sum_e\sum_{l=1}^{k-1}\delta\rho_{he}^{(l)}(t)\delta\rho_{eh'}^{(k-l)}(t), \tag{C4}$$

$$\delta\rho_{pp'}^{(k)}(t)=\sum_e\sum_{l=1}^{k-1}\delta\rho_{pe}^{(l)}(t)\delta\rho_{ep'}^{(k-l)}(t). \tag{C5}$$

Equations (C3), (C4), and (C5) may be used to iteratively compute the optical response to all orders in the external field.

APPENDIX D: THE COULOMB MATRIX ELEMENTS

Here we give the explicit form of the Coulomb term in the Hamiltonian (2.4). As indicated in Sec. II, the contribution of the off-diagonal elements of the Coulomb interaction $V_1(\begin{smallmatrix}\nu_1\nu_2\nu_3\nu_4\\ ij\end{smallmatrix})$ ($\nu_1 \neq \nu_2$ or $\nu_3 \neq \nu_4$) is small compared with the diagonal elements $V_1(\begin{smallmatrix}\nu_1\nu_1\nu_3\nu_3\\ ij\end{smallmatrix})$. We therefore neglected these elements. The Coulomb integrals $I_{ii}^{\nu_1\nu_2}$ between orbitals ϕ_{ν_1} and ϕ_{ν_1} on the same atom i,

$$I_{ii}^{\nu_1\nu_2}=\int d^3\vec{r}_x d^3\vec{r}_y |\phi_{\nu_1}(\vec{r}_x-\vec{r}_a)|^2 \frac{1}{|\vec{r}_x-\vec{r}_y|} \times |\phi_{\nu_2}(\vec{r}_y-\vec{r}_a)|^2, \tag{D1}$$

are evaluated using the Slater orbitals given in Table II[56] and given in Table III. To obtain the Coulomb integrals on different atoms i and j with the distance $r_{i,j}$, we use Ohno's formula[58,59]

$$I_{ij}^{\nu_1\nu_2}=\frac{14.397}{\sqrt{\left[\frac{2\times 14.397}{I_{ii}^{\nu_1\nu_2}+I_{jj}^{\nu_1\nu_2}}\right]^2+r_{ij}^2}}. \tag{D2}$$

The screening effect of the Coulomb potential is taken into account by the distance dependent dielectric screening $\epsilon(r)$, derived by Haken:[60]

$$\frac{1}{\epsilon(r)}=1-\left[1-\frac{1}{\epsilon_\infty}\right]\left[1-\frac{e^{-u_e r}+e^{-u_h r}}{2}\right]-\left[\frac{1}{\epsilon_\infty}-\frac{1}{\epsilon_0}\right] \times\left[1-\frac{e^{-v_e r}+e^{-v_h r}}{2}\right], \tag{D3}$$

where

$$u_i=\left(\frac{2m_i^*\Delta E}{\hbar^2}\right)^{1/2}, \quad v_i=\left(\frac{2m_i^*\omega_{LO}}{\hbar}\right)^{1/2}. \tag{D4}$$

Here ΔE is the excitation energy of an electron-hole pair on the same site (a Frenkel exciton), $\hbar\omega_{LO}$ is the energy of the LO phonons and m_i^* is the effective mass of the particle i (electron or hole). These parameters are given in Table V.

The Coulomb interaction $V_1(\begin{smallmatrix}\nu_1\nu_2\nu_3\nu_4\\ i_1 i_2\end{smallmatrix})$ is finally given by

$$V_1(\begin{smallmatrix}\nu_1\nu_2\nu_3\nu_4\\ i_1 i_2\end{smallmatrix})=\frac{1}{\epsilon(r_{i_1 i_2})} I_{i_1 i_2}^{\nu_1\nu_3}\delta_{\nu_1\nu_2}\delta_{\nu_3\nu_4}, \tag{D5}$$

where $r_{i_1 i_2}$ is the distance between atoms i_1 and i_2.

TABLE V. Parameters for CdSe used in Haken's formula for $\epsilon(r)$.

m_e^*	$0.11m_e$
m_h^*	$0.44m_h$
ϵ_∞	5.8
ϵ_0	9.3
ω_{LO}	4.0×10^{13} s^{-1}
ΔE	10 eV

APPENDIX E: MATRIX ELEMENTS OF THE DIPOLE OPERATOR

The dipole operator matrix element between orbital ν_1 on atom i and orbital ν_2 on atom j is given by

$$\vec{\mu}_{ij}^{\nu_1\nu_2}=-e\int d^3\vec{r}\,\phi_i^{*\nu_1}(\vec{r})\vec{r}\,\phi_j^{\nu_2}(\vec{r}). \tag{E1}$$

We employ Slater's approximate analytic atomic wavefunctions[56] given in Table I and Table II. Applying the TB approximation we assume:

$$\vec{\mu}_{ij}^{\nu_1\nu_2}\sim A_i^{\nu_1\nu_2}\delta_{ij}, \tag{E2}$$

where A_i may depend on the site index.

$$\vec{\mu}_{ii}^{\nu_1\nu_2}=-e\int d^3\vec{r}\,\phi_i^{*\nu_1}(\vec{r})\vec{r}\,\phi_i^{\nu_2}(\vec{r}) =-e\int d^3\vec{r}\,\phi^{*\nu_1}(\vec{r}-\vec{R}_i)\vec{r}\,\phi^{\nu_2}(\vec{r}-\vec{R}_i) =-e\int d^3\vec{r}\,\phi^{*\nu_1}(\vec{r})(\vec{r}+\vec{r}R_i)\,\phi^{\nu_2}(\vec{r}). \tag{E3}$$

Here $\vec{R}_i$ represents the location of atom i and $\vec{r}$ is the local vector in the coordinate system whose origin is at $\vec{R}_i$.

i) $\nu_1=\nu_2$. Since the wavefunctions $\phi^{*\nu_1}$ have a definite parity, $|\phi^{\nu_1}(\vec{r})|^2$ is a even function of the coordinate.

$$\int d^3\vec{r}\,|\phi^{\nu_1}(\vec{r})|^2\vec{r}=\vec{0}.$$

We then obtain the diagonal part of the matrix element of the dipole moment;

$$\vec{\mu}_{ii}^{\nu_1\nu_1}=-e\vec{R}_i. \tag{E4}$$

(ii) $\nu_1\neq\nu_2$. Because of the orthogonality of the atomic orbitals, the contribution of the second term in the parentheses of the right hand side of the last equation of (E3) is zero. The wavefunctions ϕ_{5s} and ϕ_{6s} for Cd and ϕ_{4s} and ϕ_{5s} for Se given in Table II are not orthogonal. However, their overlaps are small and can be neglected.) We then have

$$\vec{\mu}_{ii}^{\nu_1\nu_2}=-e\int d^3\vec{r}\,\phi^{*\nu_1}(\vec{r})\vec{r}\,\phi^{\nu_2}(\vec{r}). \tag{E5}$$

These elements can be evaluated analytically and are given in Table IV.

[1] A. Henglein, Chem. Rev. **89**, 1861 (1989).
[2] Y. Wang and N. Herron, J. Phys. Chem. **95**, 525 (1991).
[3] H. Weller, Angew. Chem. Int. Ed. Engl. **105**, 41 (1993).
[4] L. Brus, Appl. Phys. A **53**, 465 (1991).
[5] A. P. Alivisatos, MRS Bull. **20**, 23 (1995); Science **271**, 933 (1996).
[6] C. B. Murray, D. J. Norris, and M. G. Bawendi, J. Am. Chem. Soc. **115**, 8706 (1993).
[7] S. H. Tolbert, A. B. Herhold, C. S. Johnson, and A. P. Alivisatos, Phys.

Rev. Lett. **73**, 3266 (1994); S. H. Tolbert and A. P. Alivisatos, Science **256**, 373 (1994).
[8] R. W. Schoenlein, D. M. Mittleman, J. J. Shiang, A. P. Alivisatos, and C. V. Shank, Phys. Rev. Lett. **70**, 1014 (1993).
[9] B. O. Dabbousi, M. G. Bawendi, O. Onitsuka, and M. F. Rubner, Appl. Phys. Lett. **66**, 1316 (1995).
[10] C. R. Kagan, C. B. Murray, M. Nirmal, and M. G. Bawendi, Phys. Rev. Lett. **76**, 1517 (1996).
[11] A. Sacra, D. J. Norris, C. B. Murray, and M. G. Bawendi, J. Chem. Phys. **103**, 5236 (1995).
[12] M. Nirmal, D. J. Norris, M. Kuno, M. G. Bawendi, Al. L. Efros, and M. Rosen, Phys. Rev. Lett. **75**, 3728 (1995).
[13] U. Banin, G.Cerullo, A. A. Guzelian, C. J. Bardeen, A. P. Alivisatos, and C. V. Shank, ''Quantum confinement and ultrafast dephasing dynamics in InP nanocrystals,'' (preprint).
[14] U. Banin, A. Mews, A. V. Kadavanich, A. A. Guzelian, and A. P. Alivisatos, ''Homogeneous optical properties of semiconductor nanocrystals,'' (preprint); A. Mews, A. V. Kadavanich, U. Banin, and A. P. Alivisatos, Phys. Rev. B **53**, 13 242 (1996).
[15] V. L. Colvin, M. C. Schlamp, and A. P. Alivisatos, Nature **370**, 354 (1994).
[16] W. L. Wilson, P. F. Szajowski, and L. E. Brus, Science **262**, 1242 (1993); L. Brus, J. Phys. Chem. **98**, 3575 (1994).
[17] D. J. Norris, A. Sacra, C. B. Murray, and M. G. Bawendi, Phys. Rev. Lett. **72**, 2612 (1994).
[18] D. J. Norris and M. G. Bawendi, J. Chem. Phys. **103**, 5260 (1995).
[19] D. J. Norris, and M. G. Bawendi, Phys. Rev. B **53**, 16 338 (1996).
[20] D. J. Norris, Al. L. Efros, M. Rosen, and M. G. Bawendi, Phys. Rev. B **53**, 16 347 (1996).
[21] J. R. Heath, J. J. Shiang, and A. P. Alivisatos, J. Chem. Phys. **101**, 1607 (1994).
[22] A. Hässelbarth, A. Eychmüller, and H. Weller, Chem. Phys. Lett. **203**, 271 (1993).
[23] M. G. Bawendi, P. J. Carroll, W. L. Wilson, and L. E. Brus, J. Chem. Phys. **96**, 946 (1992); N. Nirmal, C. B. Murray, and M. G. Bawendi, Phys. Rev. B **50**, 2293 (1994).
[24] L. E. Brus, J. Chem. Phys. **80**, 4403 (1984).
[25] A. I. Ekimov, F. Kache, M. C. Schanne-Klein, D. Ricard, C. Flytzanis, I. A. Kudryavtsev, T. V. Yazeva, A. V. Rodina, and A. L. Efros, J. Opt. Soc. Am. B **10**, 100 (1993).
[26] A. L. Efros, Phys. Rev. B **46**, 7448 (1992); A. L. Efros and A. V. Rodina, Phys. Rev. B **47**, 10 005 (1993).
[27] M. V. Rama Krishna and R. A. Friesner, J. Chem. Phys. **95**, 8309 (1991).
[28] L. W. Wang and A. Zunger, J. Phys. Chem. **98**, 2158 (1994).
[29] P. E. Lippens and M. Lannoo, Phys. Rev. B **39**, 10 935 (1989); Phys. Rev. B **41**, 6079 (1990).
[30] P. E. Lippens and M. Lannoo, Semicond. Sci. Technol. **6**, A157 (1991).
[31] N. A. Hill and K. B. Whaley, J. Chem. Phys. **99**, 3707 (1993); J. Chem. Phys. **100**, 2831 (1994).
[32] N. A. Hill and K. B. Whaley, Phys. Rev. Lett. **75**, 1130 (1995); Chem. Phys. **210**, 117 (1996).
[33] Y. Z. Hu, M. Lindberg, and S. W. Koch, Phys. Rev. B **42**, 1713 (1990).
[34] K. I. Kiang, B. P. McGinnis, Y. Z. Hu, S. W. Koch, N. Peyghambarian, A. Mysyrowicz, L. C. Liu, and S. H. Risbud, Phys. Rev. B **45**, 3465 (1992).
[35] P. Ring and P. Schuck, *The Nuclear Many-Body Problem* (Springer, New York, 1980).
[36] Proceedings of the NATO Advanced Research Workshop, *Conjugated Polymeric Materials: Opportunities in Electronics, Optoelectronics, and Molecular Electronics*, NATO ASI, Series E: Applied Sciences, Vol. 182, edited by J. L. Bredás and R. R. Chance (Kluver, Dordrecht, 1990).
[37] A. Takahashi and S. Mukamel, J. Chem. Phys. **100**, 2366 (1994).
[38] S. Mukamel, A. Takahashi, H. X. Wang, and G. Chen, Science **166**, 251 (1994).
[39] G. Chen and S. Mukamel, Chem. Phys. Lett. **240**, 296 (1995).
[40] V. Chernyak and S. Mukamel, J. Chem. Phys **104**, 444 (1996).
[41] T. Meier and S. Mukamel, Phys. Rev. Lett. **77**, 3471 (1996); T. Meier,S. Tretiak, V. Chernyak, and S. Mukamel, Phys. Rev. B (in press).
[42] S. Mukamel, *Principles of Nonlinear Optical Spectroscopy* (Oxford, New York, 1995), and references therein.
[43] W. Huhn and A. Stahl, Phys. Status Solidi (B) **124**, 167 (1984).
[44] S. Schmitt-Rink, D. S. Chemla, and H. Haug, Phys. Rev. B **37**, 941 (1988).
[45] M. Lindberg and S. W. Koch, Phys. Rev. B **38**, 3342 (1988).
[46] H. Haug and S. W. Koch, *Quantum Theory of the Optical and Electronic Properties of Semiconductors*, 3rd ed. (World Scientific, Singapore, 1994), and references therein.
[47] M. Linberg, R. Binder, and S. W. Koch, Phys. Rev. A **45**, 1865 (1992).
[48] Y. Z. Hu, R. Binder, and S. W. Koch, Phys. Rev. **B** 47, 15 679 (1993).
[49] E. Binder, T. Kuhn, and G. Mahler, Phys. Rev. **B**, 50, 18 319 (1994).
[50] T. Meier, F. Rossi, P. Thomas, and S. W. Koch, Phys. Rev. Lett. **75**, 2558 (1995).
[51] P. Vogl, H. P. Hjalmarson, and J. D. Dow, J. Phys. Chem. Solids **44**, 365 (1983).
[52] M. Chamarro, G. Gourdon, P. Lavallard, O. Lublinskaya, and A. I. Ekimov, Phys. Rev. B **53**, 1336 (1996).
[53] T. Takagahara and K. Takeda, Phys. Rev. B **53**, 4205 (1996).
[54] H. Haken, *Quantenfeldtheorie des Festkörpers* (Teubner, Stuttgart, 1973).
[55] D. J. Chadi and M. L. Cohen, Phys. Status Solidi **68**, 405 (1975).
[56] J. C. Slater, Phys. Rev. **36**, 57 (1930).
[57] S. Tretiak, V. Chernyak, and S. Mukamel, Chem. Phys. Lett. **259**, 55 (1996); J. Chem. Phys. **105**, 8914 (1996).
[58] K. Ohno, Theoret. Chim. Acta **2**, 219 (1964).
[59] K. Schulten, I. Ohmine, and M. Karplus, J. Chem. Phys. **64**, 4422 (1976).
[60] H. Haken, J. Phys. Chem. Solids **8**, 166 (1959).
[61] J. C. Slater and G. F. Koster, Phys. Rev. **94**, 1498 (1954).